NANO LETTERS

2008
Vol. 8, No. 6
1771-1777

Tunneling Conductance of Amine-Linked Alkyl Chains

Emil Prodan*,† and Roberto Car‡

Department of Physics, Yeshiva University, New York, New York 10016, and Department of Chemistry and Princeton Institute for the Science and Technology of Materials, Princeton University, Princeton, New Jersey 08544

Received April 28, 2008

ABSTRACT

The tunneling transport theory developed in ref 9 (*Phys. Rev. B* 2007, *76*, 115102) is applied to molecular devices made of alkyl chains linked to gold electrodes via amine groups. Using the analytic expression of the tunneling conductance derived in our previous work, we identify the key physical quantities that characterize the conductance of these devices. By investigating the transport characteristics of three devices, containing four, six, and eight methyl groups, we extract the dependence of the tunneling conductance on the chain's length, which is an exponential decay law in agreement with recent experimental data.

Alkyl chains are among the simplest and first organic molecular chains considered in molecular electronics experiments. Despite of a large number of studies performed in the past decade, the quest for a thorough understanding of the transport characteristics of these devices is still open. Recent experiments by Venkataraman et al.,[1] and by Chen et al.,[2] in which amine groups were used as links between molecular chains and gold electrodes, reported precise measurements of the variation of the linear conductance g with the number N of methyl groups, for N ranging from 2 to 8. As expected for tunneling transport, the results showed an exponential decay of g with N: $g = g_c e^{-\beta N}$. The main novelty of these experiments is in the accurate determination of the pre-exponential factor g_c. This opens the way to measuring with great precision the effect of the contacts on the transport characteristics of organic molecular devices.[3,4]

Tunneling transport is an old subject, but only recently it was formulated in a modern framework[5–8] in which the tunneling resistance, and more precisely the exponential decay factor β, is extracted from the complex band structure of a molecular chain. This procedure extends far beyond the limitations of simple models that approximate electron tunneling in molecular devices using square potential barriers. The present authors contributed to this formalism by deriving an analytic expression for the contact conductance g_c.[9] This expression gives g_c as an overlap integral between three well-defined and physically relevant quantities: the spectral density of the device at the Fermi level, the potential perturbation of the metallic contacts on the molecular chain, and the evanescent electron waves traversing the molecular chain. Our theory provides novel insight on the electronic structure mechanisms that underlie the experiments of refs 1 and 2. In particular, we quantify the effect of the alignment of the molecular levels with the Fermi level of the metal and the effect of the chemical bonds between the link groups and the electrodes. We find that in devices based on alkyl chains, the conductance depends less sensitively than conductance in devices based on benzene rings on the Fermi alignment of the molecular levels. This is a consequence of the complex band structure of the alkyl chains, which is characterized by a large insulating gap. We also find that the contact conductance in the amine-linked alkyl chain devices is determined to large extent by the chemical contact between a single Au atom and the amine group. In addition we characterize quantitatively the lateral extent of the region relevant to tunneling transport.

Theoretical Framework. We consider a device consisting of a long but finite periodic molecular chain attached to infinite metallic electrodes. The chain is oriented along the z axis. We assume that a self-consistent Kohn−Sham calculation for the entire device has been completed. Then, the adiabatic linear conductance is given by[9]

$$g \equiv \int \mathrm{d}\,\mathbf{r}_\perp \int \mathrm{d}\,\mathbf{r}_\perp \sigma_{zz}^{\mathrm{KS}}(\mathbf{r}_\perp, z, \mathbf{r}_\perp{}', z') \qquad (1)$$

where $\sigma_{zz}^{\mathrm{KS}}(\mathbf{r}, \mathbf{r}')$ is the zz component of the Kohn−Sham conductivity tensor. The validity of this approximation was discussed in refs 9–11. As a consequence of charge continuity, the right-hand side of eq 1 is independent of the location of z and z'. In our case it is convenient to take both z and z' in the middle of the chain.

* Corresponding author, prodan@yu.edu.
† Yeshiva University.
‡ Princeton University.

10.1021/nl8012133 CCC: $40.75
Published on Web 05/20/2008

It is also convenient to treat a device consisting of chain plus leads as a strictly periodic system strongly perturbed by the leads. The Kohn−Sham potential of the system, $V_{\mathrm{eff}}(\mathbf{r})$, is not strictly periodic inside the chain, because the effect of the leads can propagate deeply into the chain. However, one can construct a strictly periodic potential $V_0(\mathbf{r})$, by replicating the portion of $V_{\mathrm{eff}}(\mathbf{r})$ that belongs to the unit cell of the chain located in the middle of the device. In the present case this cell contains two molecular CH_2 units. Then the total effective Hamiltonian $H = -\nabla^2 + V_{\mathrm{eff}}(\mathbf{r})$ can be written as (we use $\hbar = 1$, $2m = 1$, $e^2 = 2$ units)

$$H = -\nabla^2 + V_0(\mathbf{r}) + \Delta V(\mathbf{r}) \equiv H_0 + \Delta V(\mathbf{r}) \tag{2}$$

where $\Delta V(\mathbf{r}) = V_{\mathrm{eff}}(\mathbf{r}) - V_0(\mathbf{r})$. We further decompose ΔV into left and right parts relative to the midplane of the device: $\Delta V = \Delta V_{\mathrm{L}} + \Delta V_{\mathrm{R}}$. The reason for putting in evidence a periodic Hamiltonian H_0 in eq 2 is that periodic potentials are simple and lead, in particular, to a compact expression for Green's function.[12] Moreover, ref 13 showed that, whenever a periodic system is perturbed by a distant ΔV, as in the present case, one can derive a nonperturbative expression for the total Green's function, which can be used to calculate the Kohn−Sham conductivity tensor needed in eq 1. In particular, in the limit of long chains, this approach leads to the asymptotic expression[9]

$$g = \frac{1}{\pi}\frac{\Theta_{\mathrm{L}}\Theta_{\mathrm{R}}}{(\partial_k \varepsilon_k)^2} e^{2ikL} \tag{3}$$

Here k is the complex wavenumber of the evanescent Bloch solution $\psi_k(\mathbf{r})$ of the periodic Hamiltonian H_0 having minimum imaginary wavenumber and energy ε_k equal to ε_{F}, the Fermi level of the leads. The tunneling coefficient β is related to k via $\beta = 2\mathrm{Im}[k]b$, where b is the lattice constant of the chain. The contact conductance g_c is the pre-exponential factor in eq 3. The Θ_{L} coefficient is defined by

$$\Theta_{\mathrm{L}} = 2\pi i \int \mathrm{d}\mathbf{r} \int \mathrm{d}\mathbf{r}' e^{-ik(z+z')} u_{-k}(\mathbf{r}) \Delta V_{\mathrm{L}}(\mathbf{r}) \rho_{\varepsilon_{\mathrm{F}}}(\mathbf{r}, \mathbf{r}') \Delta V_{\mathrm{L}}(\mathbf{r}') u_{-k}(\mathbf{r}') \tag{4}$$

where $\mathbf{r}$ and $\mathbf{r}'$ are measured from the left end of the chain. Similarly

$$\Theta_{\mathrm{R}} = 2\pi i \int \mathrm{d}\mathbf{r} \int \mathrm{d}\mathbf{r}' e^{ik(z+z')} u_{k}(\mathbf{r}) \Delta V_{\mathrm{R}}(\mathbf{r}) \rho_{\varepsilon_{\mathrm{F}}}(\mathbf{r}, \mathbf{r}') \Delta V_{\mathrm{R}}(\mathbf{r}') u_{k}(\mathbf{r}') \tag{5}$$

where $\mathbf{r}$ and $\mathbf{r}'$ are measured from the right end of the chain. In the above expressions, the evanescent waves were factorized into exponentially and periodically varying parts, $\psi_k(\mathbf{r}) = e^{ikz}u_k(\mathbf{r})$. ρ_ε is the spectral operator, $\rho_\varepsilon = (2\pi i)^{-1}(G_{\varepsilon+i\delta} - G_{\varepsilon-i\delta})$. Its diagonal part gives the local density of states $\rho_\varepsilon(x, y, z)$ of the device. The denominator in eq 3 is the derivative with respect to k of the band energy ε_k, evaluated at ε_{F}.

Equation 3 is an asymptotic expression, valid in the limit of long chains. When the chains are finite, the conductance takes the form $g = g_c e^{-\beta N}[1 + O(e^{-\beta N})]$.[9] Taking for β the value found in the present calculations, the exponential factor $e^{-\beta N}$ is equal to 0.04, 0.007, and 0.001, respectively, for $N = 4$, 6, and 8. Thus, already chains of four monomers are well within the asymptotic regime, a result in good agreement with the experimental findings of ref 1.

Geometrical Models and Electronic Structure. We studied three devices containing four, six, and eight methyl groups, linked to gold electrodes via amine groups. In the following, these three devices will be referred to as (a), (b), and (c), respectively. The corresponding atomic configurations are shown in the first row of Figure 1. The alkyl chain has the same geometry as in refs 6 and 14. The amine groups at the two ends of the chain simply replace a methyl group, and we neglect the small difference in length between the NH and the CH bond. Indicating by A, B, and C the stacking planes in the (111) direction of face-centered cubic gold, a device consisting of an alkyl chain and two gold leads is represented schematically by

$$\mathrm{BCBCBA\text{-}NH_2\text{-}(CH_2)_{\mathit{N}}\text{-}NH_2\text{-}ACBCBC} \tag{6}$$

As shown in Figure 1 only one Au atom of the A plane is included, whereas each of the B and C planes is represented by three Au atoms. The Au−N bond length is fixed to 2.4 Å, and the Au−N−C angle is set to 109.5°. The two leads are slightly tilted relative to the alkyl chain in order to enforce the above geometrical constraints and to permit periodic

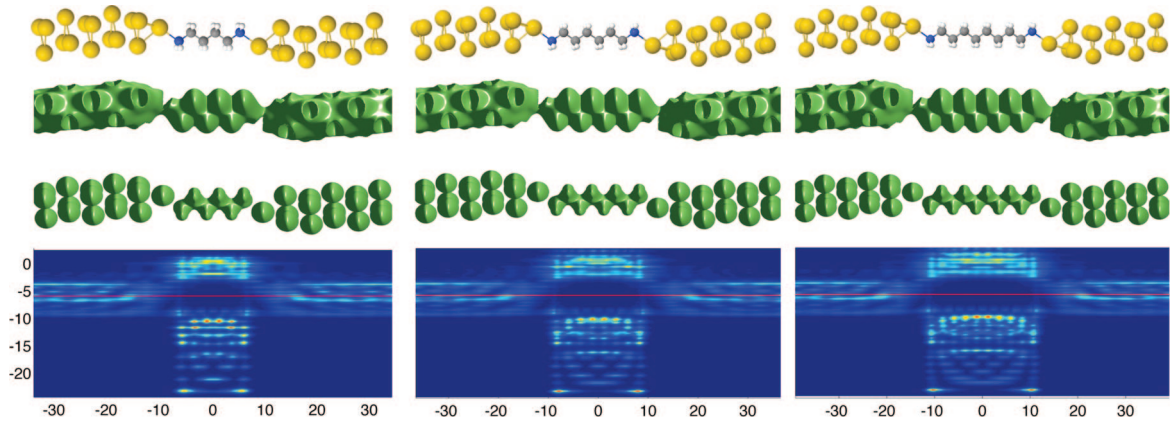

Figure 1. Atomic configurations of the molecular devices. Under each atomic configuration, the figure shows isosurfaces of the self-consistent electron density (corresponding to a value which is 1% of the maximum electron density), of the self-consistent Kohn−Sham potential (corresponding to a value which is 5% of the maximum potential), and the planar average (over xy) of the local density of states, shown as a density plot with energy (in eV) on the vertical axis and z coordinate (in a.u.) on the horizontal axis.

boundary conditions along the z direction between the left and right ends of the device. Our calculations were performed on periodic supercells containing the alkyl chain and the Au wires that represent the leads in Figure 1. The supercell dimensions (in a.u.) for the three devices were (a) 22.30 × 22.30 × 68.94, (b) 22.30 × 22.30 × 73.70, and (c) 22.30 × 22.30 × 78.45. Periodic boundary conditions were applied in all three dimensions, but in this setup periodicity along x and y is only a matter of numerical convenience because the leads (and the molecules) are well separated from their periodic replicae in the xy plane.

The equilibrium self-consistent Kohn−Sham calculations were performed with a real space pseudopotential code based on finite differences. We adopted a five-point finite difference approximation for the kinetic energy operator and used a uniform space grid with a one-dimensional spacing of 0.3656 a.u., sufficient for a good convergence of the electronic band structure. This grid is commensurate with the unit cell of the periodic alkyl chain, which is the reference system in our transport calculations. We adopted the local density approximation (LDA) for exchange and correlation using the Perdew−Zunger (PZ)[15] interpolation of the numerical electron-gas data of Ceperley and Alder.[16]

We used Troullier−Martins norm-conserving pseudopotentials[17] for all the atomic species. The pseudopotentials for C and N atoms had distinct s and p components, and we took the p pseudopotential as the local reference. Purely local pseudopotentials were used for the H and Au atoms. In the latter case only the outermost s electrons were treated explicitly, but nonlinear core corrections were included.[18] This approach overestimates the work function of gold yielding values between 6.28 and 6.70 eV depending on the surface orientation.[19] On the other hand, when the d electrons are treated explicitly, the LDA yields workfunctions close to experiment.[19] In our calculation we find a vertical ionization potential of 6.4 eV for the Au wires, which should be compared to an average experimental value of 5.4 eV for the workfunction of the Au (111) surface.[20] We will comment later on the effect of this error on the conductance.

Our real-space code yields band structures in good agreement with standard plane wave calculations. In particular, the valence band edges of an infinite alkyl chain in vacuum are located at −6.4 and −20.0 eV, respectively, and the insulating gap is equal to 5.8 eV, in good agreement with refs 14 and 22.

In Figure 1, we show the isosurface of the self-consistent electron density $n(\mathbf{r})$ corresponding to a value which is 1% of the maximum electron density. We also show the isosurface of the self-consistent potential $V_{\mathrm{eff}}(\mathbf{r})$ corresponding to a value which is 5% of the maximum potential. Here $V_{\mathrm{eff}}(\mathbf{r})$ includes Hartree, exchange-correlation, and local pseudopotential contributions. Interestingly, there are no visible differences on both isosurfaces as we move from the CH_2 units to the NH_2 end groups. Notice that to a very good approximation both $n(\mathbf{r})$ and $V_{\mathrm{eff}}(\mathbf{r})$ are periodic inside the molecular chains all the way to the first atoms of the Au contacts.

The lower panels in Figure 1 show the local density of states, averaged in the xy plane:

$$\rho_{\mathrm{av}}(z,\epsilon) = \int \rho_{\epsilon}(x,y,z)\,\mathrm{d}x\,\mathrm{d}y$$

The plots give a color map of $\rho_{\mathrm{av}}(z,\varepsilon)$ in the plane of energy ε and of position z. The Fermi level is indicated by the red line. One sees that the conducting states of the leads decay rapidly to zero inside the alkyl chain, where a spectral gap is visible. The alignment of the gap edges relative to the Fermi level is approximately, but not exactly, the same for the three devices. One can detect a slight band bending near the contacts, despite the fact that $V_{\mathrm{eff}}(\mathbf{r})$ appears to be approximately periodic all the way to the first atoms of the Au electrodes. When the energy ε is inside the spectral gap of the chain, $\rho_{\mathrm{av}}(z,\varepsilon)$ does not show any special features near the contacts. The gap is clean all the way to the first gold atoms of the electrodes, showing that no surface resonances are present.

Band Alignment. It is important to assess the accuracy of the LDA and of the available semilocal DFT approximations in the description of the level alignment at metal−molecule interfaces.[23,24] When modeling tunneling through small gap insulators, where the complex bands are parabolic, and thus depend sensitively on the energy, a relatively small change in the level alignment can affect significantly the theoretical predictions. For example, in ref 25, which used a generalized gradient approximation (GGA) treatment, the linear conductance of a device consisting of one benzene molecule linked to gold electrodes via amine groups was found to be seven times larger than the measured experimental value. However, a rigid shift of the Fermi level by 0.5 eV could restore an almost perfect agreement between theory and experiment. A different situation occurs in the case of the alkyl chains, which have a large insulating gap. The relevant complex band connecting the top of the valence bands to the bottom of the conduction bands is not parabolic but flattens away from the band edges, as illustrated in Figure 2. Thus when the Fermi level falls sufficiently far from the band edges, β becomes relatively insensitive to its precise location, suggesting that the calculated conductance could also be relatively insensitive to the DFT errors in the band alignment. We stress, however, that the connection between band alignment and conductance, although instructive, should not be taken too strictly. In fact, the Kohn−Sham levels are not quasi-particle energy levels, i.e., they do not truly correspond to observable properties. On the other hand the linear adiabatic conductance of eq 1 is a static response function which is well within the realm of ground-state DFT.

Tight-binding calculations on thiol-linked alkyl chains reported in ref 6 give a Fermi level pinned at the branch point. In our calculations, the branch point (see Figure 2) is very close to the vacuum level and, consequently, the scattering states (which were not included in the tight-binding treatment of ref 6) push the Fermi level down to about 2 eV below the branch point. As a result, the Fermi level, indicated by the red horizontal line in Figure 2, is located above the valence band edge of the alkyl chain by 3 eV. This value reflects in part the omission of an explicit treatment of the d orbitals of gold in our calculation. In a separate calculation,[21] which was performed with the plane wave pseudopotential

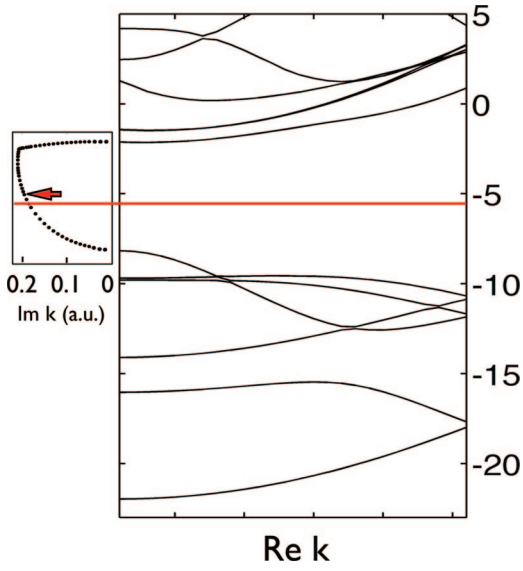

Figure 2. Real and complex band structures corresponding to the periodic potential V_0 for device (c). The horizontal line indicates the Fermi level of the device and the arrow indicates the Fermi level predicted in ref 21. The main difference between our band structure and that of an infinite periodic chain in vacuum is a rigid energy shift (see text). Only the complex bands with smallest Im[k] are shown. The energy units are eV.

code PWSCF[26] and included the d electrons of gold explicitly, we found that the Fermi level is pushed upward by 0.7 eV, to the position indicated by the arrow in Figure 2. The impact of this shift on the calculated conductance is minor, since in that energy range the complex band is relatively flat. In fact, as shown in Figure 2, an upward shift of the Fermi level by 0.7 eV leads to an increase in the value of β by about 8%. The corresponding effect on g_c should be negligible due the parabolic character of the s band of gold and the absence of surface resonances in the spectral gap. Taking only the change of β into account, the Fermi level shift would reduce the calculated conductance by factors equal to 1.49, 1.82, and 2.22, respectively, for the three devices (a−c).

Our most important observation here is that the exponential decay law of the conductance with the chain's length is only valid if the band alignment does not change with the length of the chain, because otherwise β would become a function of the chain length. The break junction experiments of refs 1 and 2 considered single chains. For an isolated chain, as opposed to a dense monolayer of molecular chains connected on both sides to planar electrodes, there is no a priori reason for the alignment to be independent of the chain's length. This is because a planar sheet of contact dipoles could be present in the case of a dense monolayer and the electrostatic effect of a planar array of dipoles would extend uniformly away from the electrode surfaces, whereas the effect of a single isolated dipole would die off with distance. In our calculations (see Figure 3), we observe a small drift of the Fermi level as the chain's length is increased. Due to the weak energy dependence of β, such a small drift does not affect appreciably the exponential law, at least for the three chains considered here.

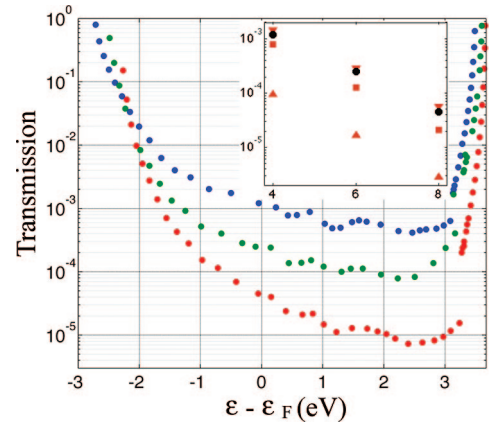

Figure 3. Transmission coefficient of the three devices (blue for device a, green for device b, and red for device c) as a function of energy relative to ε_F). The inset shows a comparison between our prediction (black dots) for the linear conductance (in units of $2e^2/h$) and the experimental data of ref 1 (red squares) and two sets of data reported in ref 2 (up and down triangles). The theoretical values were extracted from the main plot at ε_F. The experimental values were generated using the values of β and g_c reported in these references.

Table 1. β and g_c from Our Work and the Previously Reported Experimental and Theoretical Values

reference	β	g_c (kΩ)
our work (theory)	0.82	388
ref 1 (experiment)	0.91 ± 0.03	430
ref 2 (HC, experiment)	0.81 ± 0.01	350
ref 2 (LC, experiment)	0.88 ± 0.03	4044
ref 27 (theory)	0.98	140

Conductance: Numerical Results. We computed the transmission coefficient of our devices by evaluating eq 3 at several energies ε within the insulating gap, and the results are reported in Figure 3 as a function of $\varepsilon - \varepsilon_F$. The inset shows the corresponding linear conductance g of the three devices at the Fermi energy ε_F. The inset also shows experimental values taken from ref 1 and from ref 2. In the case of the latter experiment, two sets of data are reported, corresponding to high conductance (HC) and low conductance (LC) data, respectively. HC and LC data are likely to correspond to two different sets of contact geometries probed in the experiment of ref 2. By fitting our data in the inset with a straight line, we obtain a decay constant $\beta = 0.82$ and a contact resistance of 388 kΩ. These values are compared in Table 1 with the corresponding values extracted from the two cited experiments.

The agreement between our results, those of ref 1, and the HC data of ref 2 is rather good, particularly in view of the exponential dependence of the conductance on the molecular length. We also report in Table 1 the values of β and g_c obtained in a recent theoretical calculation for the same devices.[27] This work adopted contact geometries similar to ours but otherwise used a very different approach based on quantum chemical configuration interaction calculations on finite clusters. Apart from differences in the adopted electronic structure method, the most distinctive feature of our approach is that it is based on linear response theory. It is this feature that allows us to identify explicitly the various

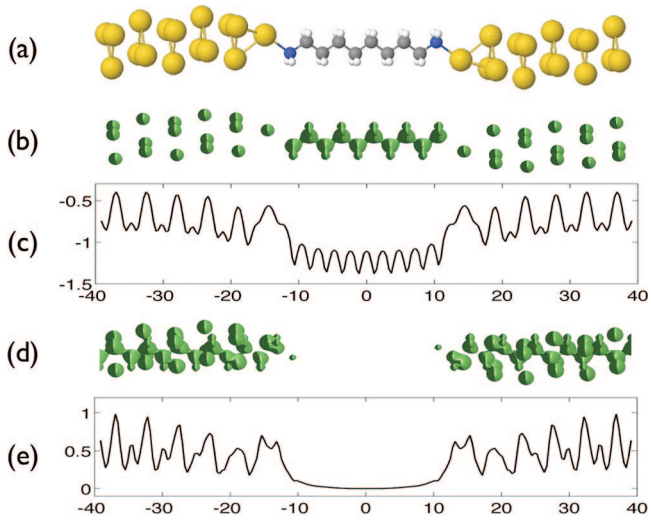

Figure 4. (a) Atomic configuration of device c. (b) An isosurface of V_{eff}. (c) Planar average of V_{eff} (with respect to the xy coordinates). (d) An isosurface of ΔV. (e) Planar average of ΔV (with respect to the xy coordinates). The energy units are Ry.

physical factors that contribute to β and g_c in the low bias limit.

In the following we explain in detail how we calculated the conductance, as it is useful to gain insight on the physics behind our results. In Figure 4 we illustrate the decomposition of V_{eff} in terms of $V_0 + \Delta V$ for device c. The second and third rows of the figure show that, within very small deviations, the self-consistent potential is periodic inside the chain. This is confirmed by the isosurface and the xy average plots of $|\Delta V|$, which both indicate that $|\Delta V|$ rapidly decreases as we move away from the contacts inside the chain. Similar results were found for the other two devices.

The complex band structure corresponding to V_0 varies slightly when different devices are considered, but overall the bands are similar to the bands of an isolated periodic chain reported in ref 14. This suggests that the main difference between V_0 and the self-consistent potential of an isolated infinite chain is a constant energy shift. Given the complex band structure of the alkyl chains, the tunneling conductance is determined by just one complex band, the one with the smallest Im[k], as discussed in refs 6 and 14. This complex band is shown in Figure 2 for device c. It was obtained by varying continuously Im[k] from 0 to its maximum value, while keeping Re[k] = 0. For each complex value of k, the spectrum of the k dependent Hamiltonian

$$H_k = -(\nabla - ik\mathbf{e}_z)^2 + V_0 + e^{-ik(z-z')}V_{\text{nonlocal}}(\mathbf{r}, \mathbf{r}') \qquad (7)$$

with periodic boundary conditions at $z = \pm b/2$, was calculated and its eigenvalues ordered according to their real parts: Re[ε_{1k}] < Re[ε_{2k}] < .... We focus, in particular, on the sixth and seventh eigenvalues ε_{6k} and ε_{7k} (which take real values, see Figure 2) and their corresponding evanescent Bloch functions ψ_{6k} and ψ_{7k}. When Im[k] = 0, ε_{6k} and ε_{7k} coincide, respectively, with the top of the valence bands and with the bottom of the conduction bands of V_0. For small Im[k], ε_{7k} originates from vacuum scattering states, but its character changes when Im[k] exceeds a certain value (see the sharp change in the complex band shown in Figure 2)

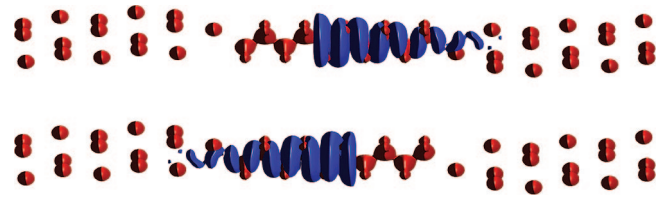

Figure 5. An isosurface plot (blue surface) corresponding to 5% of the maximum value of the evanescent Bloch functions $|\psi_{\pm k}(\mathbf{r})|$ at the Fermi energy for device c. For illustrative convenience the Bloch functions $|\psi_{\pm k}(\mathbf{r})|$ were truncated at their left/right end, respectively. For reference, we also show an isosurface plot of the effective potential (in red).

and becomes the same as that of ε_{6k}. By further increasing Im[k], the two eigenvalues move toward each other and coincide when k reaches the branch point, which is located at Im[k] = 0.21 (a.u.), in good agreement with the finding of ref 14 for an infinite alkyl chain in vacuum.

At different values of Im[k], we evaluated the conductance in eq 3 for both $\varepsilon = \varepsilon_{6k}$ and $\varepsilon = \varepsilon_{7k}$, using the corresponding evanescent Bloch functions ψ_{6k} and ψ_{7k} to compute the Θ coefficients. The evanescent Bloch functions were also used to compute the derivative $\partial_k \varepsilon_k$, making use of a Wronskian identity derived in ref 9. The spectral kernel was computed directly from the Kohn−Sham orbitals of the full device, ϕ_i, and their corresponding energies ε_i:

$$\rho_\varepsilon(\mathbf{r}, \mathbf{r}') = \sum_i \phi^*_i(\mathbf{r})\phi_i(\mathbf{r}')\delta(\varepsilon - \varepsilon_i) \qquad (8)$$

with either $\varepsilon = \varepsilon_{6k}$ or $\varepsilon = \varepsilon_{7k}$.

The Dirac-delta function was approximated by a Lorentzian distribution of half-width 0.1 eV. Convergence with the number of Au layers in the leads was checked by repeating the calculations (including the self-consistent part) for devices with two up to a maximum of five Au layers in each electrode. We found that the results are already well-converged when the leads contain only three Au layers.

Discussion. It is instructive to plot the physical quantities that enter the definition of the Θ coefficients (see eqs 4 and 5). A plot of ΔV is shown in Figure 4, and a plot of the local density of states (i.e., the diagonal part of the spectral operator) is given in Figure 1. Figure 5 shows a plot of the evanescent Bloch solutions of the periodic Hamiltonian with potential V_0, evaluated at the Fermi level, for device c. These functions are a property of the periodic Hamiltonian only, but their spatial decay is fixed by the β coefficient, which depends on the Fermi level alignment as discussed earlier. The contact conductance g_c depends on the overlap of these evanescent functions with other physical quantities, and a plot like the one in Figure 5 allows us to assess quantitatively the lateral size of the contact region that is relevant to tunneling transport. The isosurfaces in Figure 5 indicate that at least 95% of the evanescent Bloch functions are completely contained in a spatial region narrower than the lateral size of the gold wires that we use in our calculation. This does not imply that the supercell can be reduced to the small volume in which the evanescent waves have non-negligible amplitude. This is so because the other two quantities that enter the definition of the contact conductance, namely, the

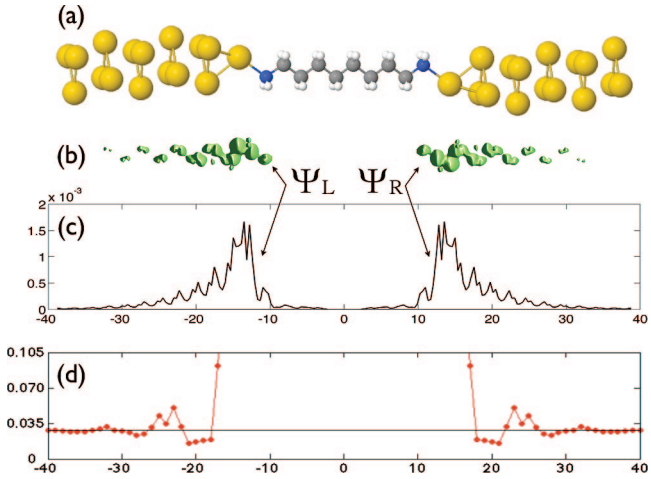

Figure 6. (a) Molecular device c. (b) An isosurface plot of $|\Psi_{L/R}(\mathbf{r})|$, corresponding to 1% of the maximum value of $|\Psi_{L/R}(\mathbf{r})|$. (c) Planar average of $|\Psi_{L/R}(\mathbf{r})|$ (with respect to the *xy* coordinates). (d) The contact conductance g_c using $|\Psi_{L/R}(\mathbf{r})|$ truncated to zero outside an interval $[-z_0, z_0]$, as function of z_0. The horizontal axes of the graphs are aligned.

spectral kernel and ΔV, are sensitive to the size of the supercell. The supercell's size should be varied until the spectral kernel and ΔV are well-converged inside the spatial region limited by the evanescent waves. For the contact geometry adopted in this paper, we have verified that this condition is well-satisfied in our calculations.

A crucial factor in our transport calculation is the fact that the overlap between the evanescent Bloch function $\psi_{\mp k}(\mathbf{r})$ and $\Delta V_{L/R}$

$$\Psi_{L/R}(\mathbf{r}) = \psi_{\mp k}(\mathbf{r})\Delta V_{L/R}(\mathbf{r}) \tag{9}$$

is exponentially localized at the left/right contacts. As a consequence, the spectral operator in eq 8 is only needed in a region near the contacts. A plot of $\Psi_{L/R}(\mathbf{r})$ for device c is shown in Figure 6. This plot allows us to understand how the different Au layers contribute to the contact conductance g_c. From panel c of Figure 6 we extract that about 62% of $\Psi_{L/R}$ comes from the region occupied by the first Au atom of the leads, i.e., the contact Au atom, 27% comes from the adjacent Au layer, and 10% comes from the remaining layers. Now, let us limit the domain of integration in the definition of the $\Theta_{L/R}$ coefficients to a finite interval $[-z_0, z_0]$. The values of g_c obtained by varying the truncation length z_0 are reported in Figure 6d. Due to inversion symmetry, we can drop the index L/R. The truncation can also be viewed as if it were caused by replacing Ψ with a Ψ' which is equal to Ψ inside and is equal to zero outside the interval $[-z_0, z_0]$. If the interval is large enough so that the difference $\delta\Psi = \Psi - \Psi'$ is small, the truncation error in g_c is given by

$$\delta g = \int \frac{\delta g}{\delta \Psi(\mathbf{r})}\delta\Psi(\mathbf{r})\, d\mathbf{r} < \max\left|\frac{\delta g}{\delta \Psi(\mathbf{r})}\right| \int_{|z|>z_0} |\Psi(\mathbf{r})|\, d\mathbf{r}$$

This shows that the plot of $\Psi_{L/R}(\mathbf{r})$ gives a measure of the convergence of g_c to its exact value. From the numbers given above, we infer that the contributions to g_c after the third Au layer are less than 10%, an estimate that is confirmed by the direct calculation shown in Figure 6d.

In conclusion, we have presented a novel and efficient approach to calculate the tunneling conductance. This scheme opens the way for first principles calculations of the conductance in devices made of long molecular chains, like, e.g., the alkyl chains in the experiments of ref 28. Our approach gives a rigorous explanation of the exponential dependence of the conductance on the molecular length and associates the exponential decay constant to a precise property of the complex band structure of a *suitably defined periodic molecular chain*. Moreover the formula for the contact conductance, i.e., the pre-exponential factor in the conductance, is relatively simple and involves overlap integrals between the evanescent waves of the periodic molecular chain and physical quantities that can be easily extracted from an equilibrium self-consistent calculation for the full device, including the electrodes and the molecular chain that connects them. Since only a region near the contacts is important, a conductance calculation can be performed on a finite model of the device, which can be conveniently done by adopting a supercell geometry like in standard surface band structure calculations. As with these calculations, care must be taken that the metal leads and the supercell are large enough for the properties near the contacts to be well converged. Finally, the formula is sufficiently simple to allow for semiquantitative estimates of the conductance without the need of numerical calculations.

For alkyl chains linked to gold electrodes via amine groups, our theoretical predictions for the tunneling conductance are in relatively good agreement with the recent experimental measurements reported in refs 1 and 2. Since our calculations used model geometries and the d electrons of the Au atoms were frozen, further, more elaborate calculations are needed to confirm the accuracy of the present results. We found the level alignment in the alkyl-based devices to be less important than one could anticipate due to the flattening of the relevant complex band away from the gap edges. Finally, we found that the contact conductance is determined mainly by the chemical link between a single atom of each gold electrode and the amine group at the corresponding end of the molecular chain.

Acknowledgment. Partial support for this work was provided by the NSF-MRSEC program through the Princeton Center for Complex Materials (PCCM), Grant DMR 0213706, and by DOE through Grant DE-FG02-05ER46201. E.P. acknowledges additional financial support from Yeshiva University.

References

(1) Venkataraman, L.; Klare, J.; Tam, I.; Nuckolls, C.; Hybertsen, M.; Steigerwald, M. *Nano Lett.* **2006**, *6*, 458.
(2) Chen, F.; Li, X.; Hihath, J.; Huang, Z.; Tao, J. *J. Am. Chem. Soc.* **2006**, *128*, 15874.
(3) Venkataraman, L.; Klare, J.; Nuckolls, C.; Hybertsen, M.; Steigerwald, M. *Nature* **2006**, *442*, 904.
(4) Cui, X.; Primak, A.; Zarate, X.; Tomfohr, J.; Sankey, O.; Moore, A.; Moore, T.; Gust, D.; Harris, G.; Lindsay, S. *Science* **2001**, *294*, 571.
(5) Mavropoulos, P.; Papanikolaou, N.; Dederichs, P. *Phys. Rev. Lett.* **2000**, *85*, 1088.
(6) Tomfohr, J.; Sankey, O. *Phys. Rev. B* **2002**, *65*, 245105.
(7) Tomfohr, J.; Sankey, O. *J. Chem. Phys.* **2004**, *120*, 1542.
(8) Fagas, G.; Kambili, A.; Elstner, M. *Chem. Phys. Lett.* **2004**, *389*, 268.
(9) Prodan, E.; Car, R. *Phys. Rev. B* **2007**, *76*, 115102.
(10) Kamenev, A.; Kohn, W. *Phys. Rev. B* **2001**, *63*, 155304.
(11) Koentopp, M.; Burke, K. *Phys. Rev. B* **2006**, *73*, 121403.

(12) Prodan, E. *Phys. Rev. B* **2006**, *73*, 035128.
(13) Prodan, E.; Kohn, W. *Proc. Natl. Acad. Sci. U.S.A.* **2005**, *102*, 11635.
(14) Picaud, F.; Smogunov, A.; Corso, A. D.; Tosatti, E. *J. Phys.: Condens. Matter* **2003**, *15*, 3731.
(15) Perdew, J.; Zunger, A. *Phys. Rev. B* **1981**, *23*, 5048.
(16) Ceperley, D.; Alder, B. *Phys. Rev. Lett.* **1980**, *45*, 566.
(17) Troullier, N.; Martins, J. *Phys. Rev. B* **1991**, *43*, 1993.
(18) Louie, S.; Froyen, S.; Cohen, M. *Phys. Rev. B* **1982**, *26*, 1738.
(19) Fall, C.; Binggeli, N.; Baldereschi, A. *Phys. Rev. B* **2000**, *61*, 8489.
(20) Hansson, G.; Flodstrom, S. *Phys. Rev. B* **1978**, *18*, 1572.
(21) Wang, J.; Prodan, E.; Selloni, A.; Car, R. In preparation, 2008.
(22) Montanari, B.; Jones, R. *Chem. Phys. Lett.* **1997**, *272*, 347.
(23) Neaton, J.; Hybertsen, M.; Louie, S. *Phys. Rev. Lett.* **2006**, *97*, 216405.
(24) Quek, S.; Neaton, J.; Hybertsen, M.; Kaxiras, E.; Louie, S. *Phys. Status Solidi* 2006*243*, 2048.
(25) Quek, S.; Venkataraman, L.; Choi, H.; Louie, S.; Hybertsen, M.; Neaton, J. *Nano Lett.* **2007**, *7*, 3477.
(26) Baroni, S.; Corso, A. D.; de Gironcoli, S.; Giannozzi, C. C. P.; Ballabio, G.; Scandolo, S.; Chiarotti, G.; Focher, P.; Pasquarello, A.; Laasonen, K. 2008, URL http://www.pwscf.org.
(27) Fagas, G.; Greer, J. *Nanothechnology* **2007**, *18*, 424010.
(28) Salomon, A.; Boecking, T.; Chan, C. K.; Amy, F.; Girshevitz, O.; Cahen, D.; Kahn, A. *Phys. Rev. Lett.* **2005**, *95*, 266807.

NL8012133